Effect of alkyl substituents: 5,15-bis(trimethylsilylethynyl)- vs 5,15-bis(triisopropylsilylethynyl)-tetrabenzoporphyrins and their metal complexes

Kohtaro Takahashi,[a] Naoya Yamada,[b] Daichi Kumagai,[b] Daiki Kuzuhara,[a] Mitsuharu Suzuki,[a] Yuji Yamaguchi,[b] Naoki Aratani,[a] Ken-ichi Nakayama,[b,d,*] and Hiroko Yamada[a,c,*]

Dedicated to Professor Shunichi Fukuzumi on the occasion of his 65th birthday and his retirement from Osaka University.

[a] *Graduate School of Materials Science, Nara Institute of Science and Technology, 8916-5, Ikoma, Nara 630-0192, Japan.* [b] *Department of Organic Device Engineering, Graduate School of Science and Engineering, Yamagata University, Yonezawa 992-8510, Japan,* [c] *CREST, Japan Science and Technology Agency (JST), 4-1-8 Honcho, Kawaguchi, Saitama 332-0012, Japan*

Received date (to be automatically inserted after your manuscript is submitted)
Accepted date (to be automatically inserted after your manuscript is accepted)

ABSTRACT: The copper(II), nickel(II), etc. complexes of 5,15-bis(trimethylsilylethynyl)tetra benzoporphyrin (**TMS-H_2BP**) and 5,15-bis(triisopropylsilylethynyl)tetrabenzoporphyrin (**TIPS-H_2BP**) have been prepared from the corresponding bicycle[2.2.2]octadiene(BCOD)-fused precursors by the retro-Diels–Alder reaction. X-ray diffraction (XRD) analyses show that **TMS-H_2BP** and its metal complexes of zinc(II) (**TMS-ZnBP**) and copper(II) (**TMS-CuBP**) adopt flat molecular conformations and form herringbone-type packing structures in the single crystalline state. **TIPS-H_2BP** and the zinc(II) and copper(II) complexes (**TIPS-ZnBP** and **TIPS-CuBP**) are similar to the TMS derivatives in molecular conformation, but these TIPS derivatives form one-dimensional slipped-stack structures. The nickel complexes **TMS-NiBP** and **TIPS-NiBP** have U-shaped structures because of the small size of nickel(II) ion. Solution processed organic thin-film transistors of the benzoporphyrins were fabricated and **TMS-H_2BP** showed the highest hole mobility of 0.11 $cm^2.V^{-1}.s^{-1}$. Bulk heterojunction organic solar cells based on **TMS-** or **TIPS-H_2BP** and their metal complexes as p-type and $PC_{71}BM$ as n-type materials were fabricated by solution process. Atomic force microscopy and thin-film XRD measurements indicated that the film crystallinities were increased by raising the annealing temperature over 180 ºC or by changing the substituents from triisopropylsilyl to trimethylsilyl. The best power-conversion efficiency (PCE) of 1.49% was achieved with **TMS-ZnBP** by annealing at 180 ºC with a moderate crystallinity and smooth surface.

KEYWORDS: Benzoporphyrin, Metal complexes, Crystal structure, Organic solar cells.

*Correspondence to: Hiroko Yamada, e-mail: hyamada@ms.naist.jp, tel: + 81-743-72-6042.

INTRODUCTION

Organic semiconducting materials have attracted much attention for the development of organic electronics such as organic thin-film transistors (OTFTs) and organic solar cells (OSCs). These organic electronic devices are expected to be flexible, light-weight, large area and low cost. Recently, high mobilities of over 10 $cm^2.V^{-1}.s^{-1}$ have been attained in OTFTs, which are close to or over the performances of amorphous silicon devices [1, 2]. The power-conversion efficiencies of OSCs have been reported to reach almost 10% with single and tandem systems using polymers as active layers [3]. Tetrabenzoporphyrin (**BP**) has been reported as one of the excellent organic semiconducting materials. However, the solubility of **BP** is low in common organic solvents, and thus **BP** is not compatible with solution-based deposition processes. In order to apply **BP** to solution-process, Ono and his colleagues have developed a soluble precursor of **BP**, bicyclo[2.2.2]octadiene-fused (or annulated) porphyrin (**CP**), which is soluble in common organic solvents such as chloroform, toluene and chlorobenzene [4]. The precursor **CP** can be quantitatively converted to **BP** upon heating through the retro Diels–Alder reaction (Fig. 1) in solution and in the solid state without chemical reagents and purification. This thermal conversion method thus has allowed us not only to synthesize π-expanded porphyrins and related compounds [5], phthalocyanines [6], BODIPYs [7], isothianaphthenes [8], thioindigo [9] and acenes [10], but also to apply the materials to solution-processed OTFTs and OSCs. Ono, Kanicki, and coworkers have achieved a carrier mobility of 0.1 $cm^2.V^{-1}.s^{-1}$ in a top-gate-bottom-contact OTFT device [11]. In addition, the precursor method enables fabrication of multi-layer organic films by solution process owing to the insolubilization of thin films after the thermal conversion. Using this "precursor approach", Nakamura et al. fabricated p–i–n-type OSC devices based on **BP** as p-type material and bis(dimethylphenylsilylmethyl)[60]fullerenes (SIMEF) as n-type material to achieve the maximum photo-conversion efficiency (PCE) of 5.2% [12]. More recently, we have reported the synthesis of a **BP**–fullerene dyad for use as the inter (i)-layer material in p–i–n-type OSCs, in which we obtained PCEs up to 1.98% [13].

To improve the performance of organic electronic devices, molecular design of semiconducting materials is among the most important considerations. Pentacene is one of the most promising organic semiconducting materials showing good carrier mobilities of over 1 $cm^2.V^{-1}.s^{-1}$ in OTFT devices, but it is hardly soluble in common organic solvents and unstable in ambient conditions. In contrast, 6,13-triisopropylsililethynyl-pentacene (TIPS-PEN) represents a good solubility and chemical stability owing to the introduction of the bulky triisopropylsilyl (TIPS)-ethynyl groups to the most reactive 6,13-positions. The pristine pentacene packs to form a herringbone motif, while TIPS-PEN forms a two-dimensional-slipped-stack column structure [14]. TIPS-PEN-based OTFTs show superior carrier mobilities of up to 11 $cm^2.V^{-1}.s^{-1}$ in solution-processed single-crystalline film [15]. Motivated by these results, various TIPS and related trialkylsilyl substituted acene derivatives have been developed as organic FET materials [16].

Based on these precedent contributions, we have designed and synthesized 5,15-bis(trimethylsilylethynyl) tetrabenzporphyrin (**TMS-H_2BP**), 5,15-bis(triisopropylsilylethynyl)tetrabenzporphyrin (**TIPS-H_2BP**) and their zinc complexes [17]. Trialkylsilylethynyl groups were introduced to the 5- and 15-positions of **BP** to expand π-conjugation effectively. **TMS-H_2BP** and **TIPS-H_2BP** were prepared by the retro Diels–Alder reaction of BCOD-fused 5,15-bis(trimethylsilylethynyl)porphyrin (**TMS-H_2CP**) and 5,15-bis(triisopropylsilylethynyl)porphyrin (**TIPS-H_2CP**), respectively. The absorption of **TMS-H_2BP** is redshifted as compared to **BP** and its absorption edge reaches 710 nm. Such a redshift is favorable for OSC materials, and a similar redshift was observed for **TIPS-H_2BP**. At the same time, the solubility and crystal structures are different depending on the introduced substituent. Herein, we will describe the synthesis, optical properties, electrochemical properties and crystal structures of zinc(II), copper(II) and nickel(II) complexes of **TMS-H_2BP** and **TIPS-H_2BP** in order to discuss the substituent effect of trimethylsilyl (TMS) and TIPS

groups on **BP**. The performances of OTFT and bulk heterojunction (BHJ) OSC devices of **TMS-H_2BP**, **TIPS-H_2BP** and their zinc and copper complexes as p-type materials and [6,6]-phenyl C_{71} butyric acid methyl ester ($PC_{71}BM$) as an n-type material will be also discussed.

RESULTS AND DISCUSSION

Synthesis and characterization of TMS-BP and TIPS-BP metal complexes

TMS-H_2CP, **TMS-H_2BP**, **TIPS-H_2CP** and **TIPS-H_2BP** and the corresponding zinc(II) complexes were prepared according to the literature [17a–c]. The synthesis of metal complexes of **TMS-BP** and **TIPS-BP** is shown in Scheme 1. The copper and nickel complexes of **TMS-CP** and **TIPS-CP** were synthesized from **TMS-H_2CP** and **TIPS-H_2CP** by general metal insertion methods. **TMS-H_2CP** and **TIPS-H_2CP** were reacted with $Cu(OAc)_2{\cdot}H_2O$ in $CHCl_3$ and MeOH to give **TMS-CuCP** in 84% and **TIPS-CuCP** in 91% yields. The nickel complexes were also prepared from **TMS-H_2CP** and **TIPS-H_2CP** through the reactions with $Ni(OAc)_2{\cdot}4H_2O$ in $CHCl_3$ and MeOH, by which **TMS-NiCP** and **TIPS-NiCP** were obtained in 87% and 93% yields, respectively. The thermal conversion of copper and nickel complexes of **TMS-CP** and **TIPS-CP** was analyzed by thermogravimetric analysis (TGA) with a heating rate of 10 ºC.min^{-1} under a nitrogen atmosphere (Fig. 2). The mass loss of all metal complexes started atf around 150 ºC and finished at around 200 ºC. The observed mass loss of 12.8% for **TMS-CuCP** is in agreement with the calculated value of 12.8% for the loss of the four ethylene units per molecule. The mass loss for **TMS-NiCP** (12.9%) and **TIPS-NiCP** (10.2%) are also in agreement with the calculated values of 12.8% and 10.8%. On the other hand, the observed mass loss of **TIPS-CuCP** is 19.7%, which is in consistent with the loss of four ethylene molecules and a chloroform molecule per one **TIPS-CuCP** molecule (calculated value: 19.9%). The TGA results suggested that the precursor **CP**s could be converted to the corresponding **BP**s quantitatively by heating at 200 ºC in the solid state. The **TMS-CuBP** and **TMS-NiBP** exhibited low solubilities in common organic solvents, while **TIPS-CuBP** and **TIPS-NiBP** were soluble in halogenated solvents, THF and toluene. The structures of **TMS-NiBP** and **TIPS-NiBP** were characterized by ^{1}H and ^{13}C NMR specrtroscopy, high-resolution mass spectrometry (HRMS) and single-crystal X-ray diffraction (XRD) analysis. **TMS-CuBP** and **TIPS-CuBP** were also characterized by HRMS and single-crystal XRD analysis.

Photophysical and electrochemical properties

The UV–vis absorption spectra of **TMS-BP**s in DMF and **TIPS-BP**s in CH_2Cl_2 are shown in Fig. 3. The obtained optical data are summarized in Table 1. We previously reported the absorption of **TMS-H_2BP, TMS-ZnBP** [17c], **TIPS-H_2BP** and **TIPS-ZnBP** [17a] in CH_2Cl_2. **TMS-H_2BP** shows peak top of the Soret-band at 462 nm and the longest wavelength of Q-band at 711 nm and **TIPS-H_2BP** shows at 460 and 710 nm. The absorption spectra of **TMS-BP**s and **TIPS-BP**s are redshifted from **TMS-CP**s and **TIPS-CP**s because of the π-expansion (Figs. S1). The Soret band peaks of metal porphyrins are almost the same as those of free-base porphyrins, but the longest Q-band peaks are blueshifted compared to the free-base porphyrins.

To investigate the electrochemical properties of **TIPS-H_2BP** and its metal complexes, we performed the cyclic voltammetry (CV) and differential pulse voltammetry (DPV) in CH_2Cl_2 with 0.1 M *n*-Bu_4NPF_6 as an electrolyte at room temperature. The results are shown in Fig. 4 and Table 1. The electrochemical properties of **TMS-BP** metal complexes could not been measured because of the insolubility. The reversible three oxidation peaks were observed for **TIPS-H_2BP** (0.18, 0.22 and 0.48 V vs. ferrocene/ferrocenium), **TIPS-CuBP** (0.06, 0.23 and 0.68 V), **TIPS-NiBP** (0.17, 0.22 and 0.37 V) and two oxidation peaks were observed for **TIPS-ZnBP** (0.07 and 0.59 V) while the reversible two reduction peaks were observed for **TIPS-H_2BP** (–1.42 and –1.81 V), **TIPS-CuBP** (–1.34 and –1.48 V), **TIPS-NiBP** (–

1.30 and –2.01 V) and **TIPS-ZnBP** (–1.64 and –2.06 V). The first and second oxidation peaks of **TIPS-H_2BP**, **TIPS-CuBP** or **TIPS-NiBP** correspond to one electron oxidation in total, and the ratio of the two peaks changes depending on the concentration of the sample (Fig. S2). We assume that the first oxidation potential belongs to the formation of dimeric cation radical and the second peak is corresponding to the oxidation to monomeric cation. The third peak of **TIPS-H_2BP**, **TIPS-CuBP** and **TIPS-NiBP** is one electron oxidation and corresponds to the second oxidation of BP compounds. This phenomenum was also observed for a BP-C_{60} dyad [13].

Crystal structures of TMS-BP and TIPS-BP metal complexes

Single crystals of **TMS-H_2BP**, **TMS-ZnBP**, **TMS-CuBP** and **TMS-NiBP** suitable for X-ray analysis were obtained by recrystallization in *o*-dichlorobenzene (**TMS-H_2BP**, **TMS-ZnBP** and **TMS-CuBP**) or slow diffusion of heptane into a chlorobenzene solution (**TMS-NiBP**). **TMS-H_2BP** adopts a sigmoidal-shape in the single-crystalline state and is packed in one-dimensional slipped-stack structures (Fig. 5a). The neighboring columns are arranged to form a herringbone motif which is different from **TIPS-H_2BP** which form a one-dimensional columnar array. The distance associated with the π–π stacking between porphyrin cores is 3.208 Å. **TMS-ZnBP** and **TMS-CuBP** afforded similar herring-bone-type packing structures comprising of sigmoidal-shaped molecules. The shortest distance between neighboring porphyrin cores are 3.182 Å for **TMS-ZnBP** and 3.213 Å for **TMS-CuBP** (Figs. 5b and 5c). On the other hand, the BP framework in **TMS-NiBP** adopts a saddle-shaped conformation reflecting the small radius of nickel(II) atom in comparison with the cavity size of porphyrin (Fig. 5d). The intramolecular C5–C15 distances are 6.657(2) and 6.656(3) Å, and the TMS substituents orient to the same direction so that the overall molecular conformation is V-shaped when viewed from the side. Molecules of **TMS-NiBP** form a face-to-face dimeric motif, in which the two molecules are stacked orthogonally with their curved porphyrin surfaces fitting well to each other. Two chlorobenzene molecules are located in the unit cell to occupy the space between the face-to-face dimeric motifs. The TMS groups of each molecule are oriented toward its partner in the dimeric structure. The associated Ni–Ni distance in the dimer is 3.4524(3) Å. Neighboring dimers are related by an inversion center to form a slipped-stack structure extending along the <0 $\bar{1}$ 1> direction.

Single crystals of **TIPS-ZnBP** and **TIPS-CuBP** were obtained by slow diffusion of heptane into a chlorobenzene solution and by slow diffusion of methanol into a chloroform solution, respectively (Figs. 6a and 6b). **TIPS-ZnBP** and **TIPS-CuBP** have a planar benzoporphyrin core and two ethynyl groups bent from the benzoporphyrin plane sigmoidally as similar to the case of **TIPS-H_2BP**. In the packing structures of **TIPS-ZnBP** and **TIPS-CuBP**, molecules form a triad-like structures where the molecules are stacked orthogonally. The minimum plane-to-plane distance of each molecule is 3.250 Å for both **TIPS-ZnBP** and **TIPS-CuBP**, which distance is shorter than that of **TIPS-H_2BP** (3.295 Å) [17a]. The triad units are packed parallel to make one-dimensional slip-stacked structures with the plane-to-plane distances of 3.082 Å for **TIPS-ZnBP** and 3.113 Å for **TIPS-CuBP**, respectively. Single crystals of **TIPS-NiBP** were obtained by slow diffusion of ethanol into a 1,2-dichloroethane solution. The crystal structure of **TIPS-NiBP** is similar to **TMS-NiBP** (Fig. 6c). **TIPS-NiBP** molecules show a saddle-shaped comformation with the intramolecular C5–C15 distances are 6.645(2) or 6.671(2) Å, and form a face-to-face dimeric motif. The curved porphyrin surfaces are fitted well to each other, but TIPS groups of each molecule are oriented against its partner in the dimeric structure. The associated Ni–Ni contact is 3.7632(3) Å.

Fabrication and evaluation of OTFTs

We have fabricated OTFT devices utilizing the free-base and the corresponding zinc(II) and copper(II) complexes of **TMS-BP** and **TIPS-BP** to investigate the effect of the substituent structure and metalation on the performance of OTFT

devices. The **TMS-BP** or **TIPS-BP** films were fabricated by heating thin-films which were fabricated by spin-coating of the precursors, **TMS-CP** or **TIPS-CP**, on n-doped Si substrates followed by heating. Bottom-gate-top-contact structures were by evaporating the Au source and drain electrodes on the organic film. Performance parameters of each OTFT device estimated from the saturation regime are summarized in **Table 2**. The best performance was obtained with **TMS-H_2BP**, which gave a hole mobility (μ_{FET}) of 0.11 $cm^2.V^{-1}.s^{-1}$ with an on/off ratio was 2.4×10^6. The output and transfer curves of this device are shown in Fig. 7. The XRD patterns of the films heated at 180 °C suggested the edge-on configuration for these films (Fig. S6)

Fabrication and evaluation of OSCs

We have also fabricated OSCs utilizing the free-base and the corresponding zinc(II) and copper(II) complexes of **TMS-BP** and **TIPS-BP** as p-type materials with $PC_{71}BM$ as n-type material to investigate the effect of the substituent structure and metalation on the performance of OSC devices. To fabricate **TMS-** and **TIPS-BP**-based OSCs, we have initially investigated the ionization energy of thin-films on ITO-glass substrates by photoelectron spectroscopy in air to estimate the HOMO levels (E_{HOMO}) of materials. The ionization energies are 5.22 eV for **TMS-H_2BP**, 5.25 eV for **TMS-ZnBP**, 5.10 eV for **TMS-CuBP**, 5.24 eV for **TIPS-H_2BP**, 5.37 eV for **TIPS-ZnBP** and 4.88 eV for **TIPS-CuBP** (Table 1 and Fig. S3). The LUMO levels (E_{LUMO}) were estimated by adding the optical bandgaps to the IPs. The optical bandgaps were determined from the absorption onset of the thin-films (Table 1 and Fig. S4). The LUMO levels were calculated to be –3.61 eV for **TMS-H_2BP**, –3.62 eV for **TMS-ZnBP**, –3.49 eV for **TMS-CuBP**, –3.61 eV for **TIPS-H_2BP**, –3.76 eV for **TIPS-ZnBP** and –3.26 eV for **TIPS-CuBP**. The typical OPV structure was glass/ITO/PEDOT:PSS (30 nm)/**TMS-** or **TIPS-BP**:$PC_{71}BM$/BCP (7 nm)/Al (100 nm). Active layers were deposited by spin-coating (2500 rpm for **TMS-CP**s or 800 rpm for **TIPS-CP**s) of a solution containing a precursor (**TMS-CP**s or **TIPS-CP**s) and $PC_{71}BM$ (1:1 (w/w)) in a chloroform solution for **TMS-CP**s (20 $mg.mL^{-1}$) or a mixture of chloroform:chlorobenzene (1:1(v/v)) solution for **TIPS-CP**s (10 $mg.mL^{-1}$). Each the deposited film was then heated at 160, 180 or 200 °C for 30 min to generate the corresponding benzoporphyrin *in situ*. It is known that the thermal conversion temperature largely affects the device properties because of the change in film morphology and crystallinity [19].

The *J–V* curves of the devices having **TMS-H_2BP**:$PC_{71}BM$ or **TIPS-H_2BP**:$PC_{71}BM$ as active layer are shown in Figs. 8a and 9a. The values of short circuit current density (J_{SC}), open circuit voltage (V_{OC}), fill factor (FF), and power conversion efficiency (PCE) are summarized in Table 3. When the **TMS-H_2BP**:$PC_{71}BM$ film was annealed at 160 ºC, a PCE of 0.33% was obtained. By increasing the annealing temperature to 180 ºC, PCE was improved to 1.09% with J_{SC} = 5.07 $mA.cm^{-2}$, V_{OC} = 0.48 V and FF = 0.40. However, further increase of the annealing temperature to 200 ºC resulted in a decreased PCE of 0.47%. The **TIPS-H_2BP**:$PC_{71}BM$ system showed a similar tendency to **TIPS-H_2BP**:$PC_{71}BM$ and the highest PCE of 1.02% was obtained by annealing at 180 ºC associated with J_{SC} = 5.22 $mA.cm^{-2}$, V_{OC} = 0.61 V and FF = 0.28. The other annealing temperatures (160 and 200 ºC) gave lower PCE values (0.57% and 0.19%). The **TMS-H_2BP**:$PC_{71}BM$ and **TIPS-H_2BP**:$PC_{71}BM$ devices are comparable in J_{SC} and FF values, while the V_{OC} values are considerably different. The external quantum efficiency (EQE) (Figs. 8b and 9b) of the devices prepared by heating at 180 ºC is higher as compared to those obtained by heating at 160 and 200 ºC, although the absorption spectra of the blend films are similar between the 180 and 200 °C devices (Figs. 8d and 9d).

Active-layer structures of these devices were investigated by out-of-plane XRD and tapping-mode atomic force microscopy (AFM). Figs. 8c and 9c show XRD patterns of the **TMS-H_2BP**:$PC_{71}BM$ and **TIPS-H_2BP**:$PC_{71}BM$ blend films annealed at 160, 180, and 200 ºC. Diffraction peaks are observed at 2θ = 5.43º and 5.44º for the **TMS-H_2BP**:$PC_{71}BM$ blend films annealed at 180 and 200 ºC, respectively. In the case of **TIPS-H_2BP**:$PC_{71}BM$ films annealed at 180 and 200 ºC, diffraction peaks are observed at 5.45º and 5.50º, respectively. These peaks correspond to

the (001) diffraction of **TIPS-H_2BP** considering the corresponding peak observed for a **TIPS-H_2BP** neat film (Fig. S6b). The peak intensity increased with raising the annealing temperature from 180 to 200 ºC. The film annealed at 160 ºC showed no specific diffraction peaks. This observation implies that **TMS-H_2BP** and **TIPS-H_2BP** films become crystalline over 180 ºC, while the annealing at 160 ºC affords amorphous films. The similarity between the absorption spectra of the films annealed at 180 and 200 ºC is in agreement with the results of XRD. Fig. 8e–g and Fig. 9e–g show the AFM images of **TMS-H_2BP**:$PC_{71}BM$ and **TIPS-H_2BP**:$PC_{71}BM$ blend films. The **TMS-H_2BP**:$PC_{71}BM$ blend films show large domains at all annealing temperatures. These phase separation is promoted by increasing the annealing temperature. In particular, domains as large as 1 μm and large cracks were observed for the film annealed at 200 ºC. On the contrary, the **TIPS-H_2BP**:$PC_{71}BM$ blend films annealed at 160 and 180 ºC show smooth surface with smaller roughness, indicating the formation of micro-domains. In the case of the film annealed at 200 ºC, cracks were found on the surface. As the results of XRD, the higher crystallinity films of **TMS-H_2BP** and **TIPS-H_2BP** were obtained by annealing at 200 ºC, and these crystalline films have large grains. In general, the organic materials have the exciton diffusion length within 20–30 nm. To attain the high PCE values, efficient charge separation is necessary and the grain size should be in the same order as the exciton diffusion length. Therefore, the larger grain size leads to lower PCEs [20]. The film annealed at 180 ºC has the highest PCE owing to the smooth surface and moderate crystallinity of **TMS-H_2BP** and **TIPS-H_2BP**. These results indicate that the bulky TIPS groups and moderate annealing temperature inhibited the growth of large domains in blend films with $PC_{71}BM$.

The OSC using **TMS-ZnBP** or **TIPS-ZnBP** as p-type material with $PC_{71}BM$ as an n-type material were also fabricated. The results are summarized in Table 3, Figs. S7a and S7b. **TMS-ZnBP** and **TIPS-ZnBP** showed the best performances with the annealing temperature at 180 ºC. The J_{SC} and FF values of **TMS-ZnBP** were improved compared to **TMS-H_2BP**, and a PCE of 1.49% was attained. The V_{OC} value of **TMS-ZnBP** was comparable to **TMS-H_2BP**, although the E_{HOMO} of **TMS-ZnBP** is lower than that of **TMS-H_2BP**. The increase in J_{SC} is probably due to form the face-on π-π stacking of **TMS-ZnBP** in **TMS-ZnBP**:$PC_{71}BM$ films (180 and 200 °C). This is indicated by the observation peaks at 2θ = 28.5 and 28.6° (d = 3.13 and 3.12 Å) in the XRD patterns as shown in Fig. S6b. These peaks correspond to the distance of π–π stacking as supported by the crystal structure of **TMS-ZnBP** (Fig. 5b). **TIPS-ZnBP** also showed the improvement of the PCE compared to **TIPS-H_2BP**, and the 1.13% of PCE was attained.

The OSC using **TMS-CuBP** or **TIPS-CuBP** as p-type material with $PC_{71}BM$ as an n-type material were also fabricated. The copper porphyrins are known to exhibit short fluorescence lifetimes compared with the free-base porphyrins and are not suitable for the OSC, since the exciton diffusion length becomes shorter [21]. The results are summarized in Table 3 and Figs. S7c and S7d. The best annealing temperature was 160 ºC and the PCE values are 0.72 and 0.86% for **TMS-CuBP** and **TIPS-CuBP**, respectively. **TMS-CuBP** and **TIPS-CuBP** single films are crystalline (Fig. S4f), but the crystallinity of the blend films with $PC_{71}BM$ are lower than **H_2BP** and **ZnBP** films. The AFM images of **TMS-CuBP**:$PC_{71}BM$ blend films showed larger domains for the films annealed at 180 and 200 °C, although the XRD patterns showed small peaks. The AFM images of **TIPS-CuBP**:$PC_{71}BM$ blend films look smooth and amorphous. These will be one of the reasons why the J_{SC} of the devices with **TMS-CuBP** and **TIPS-CuBP** are relatively low.

CONCLUSION

We have succeeded in the preparation of the **TMS-** and **TIPS-BP** metal complexes by the retro Diels–Alder reaction of the corresponding precursors, **TMS-** and **TIPS-CP**, respectively. **TMS-** and **TIPS-BP**s exhibited very similar absorption properties with little effects from the TMS- and TIPS-groups. We revealed that the two alkylsilyl groups induced the different crystal structures. **TMS-H_2BP**, **TMS-ZnP** and **TMS-CuBP** showed the herringbone-type packing

structures, while **TIPS-H_2BP**, **TIPS-ZnP** and **TIPS-CuBP** showed the one-dimensional slip stacked structures. OTFT devices of these benzoporphyrins were fabricated by solution process and the best performance was obtained for **TMS-H_2BP** with a μ_{FET} of 0.11 $cm^2.V^{-1}.s^{-1}$. The BHJ-type OSCs based on **TMS-H_2BP** or **TIPS-H_2BP** with $PC_{71}BM$ were also fabricated. The best performance among these OSC systems was obtained with a **TMS-H_2BP**:$PC_{71}BM$ blend film annealed at 180 ºC with a PCE of 1.09%. The film structures evaluated by the AFM and XRD measurements suggested the critical effect of the annealing temperature to the film structure and thus the device performance. By annealing at 180 ºC, the crystallinity of **TMS-H_2BP** and **TIPS-H_2BP** was increased as opposed to annealing at 160 °C which resulted to the formation of amorphous films. However, annealing at 200 ºC promoted large phase separation and cracking to provide the considerably lower PCEs. The films annealed at 180 ºC have moderate crystallinities and smooth surfaces, and are suitable for OSC devices in the case of **TMS-H_2BP** and **TIPS-H_2BP**. The BHJ OSC devices based on zinc(II) and copper(II) complexes as p-type materials were also fabricated. The blend films of **TMS-ZnBP** or **TIPS-ZnBP** and $PC_{71}BM$ showed better molecular orientations, and afforded improved of the OSC performances as compared to free-base and copper(II) complex. Investigations of a wider variety of benzoporphyrin derivatives with different substituents are in progress, with the aim of achieving further improved performance in benzoporphyrin-based OSCs.

EXPERIMENTAL

General

^1H NMR and ^{13}C NMR spectra were recorded on a JEOL ECX 400P spectrometer at ambient temperature using tetramethylsilane as an internal standard. ESI mass spectra were measured on a JEOL JMS-700 spectrometer. UV–vis spectra were measured on a JASCO UV/VIS/NIR spectrophotometer V-570. All solvents and chemicals were reagent grade quality, obtained commercially and used without further purification. For spectral measurements, spectral grade solvents were purchased from Nacalai Tesque Inc. X-ray crystallographic data were recorded at 103 K (**TMS-H_2BP**, **TMS-ZnBP**, **TMS-CuBP**, **TMS-NiBP**) and 123 K (**TIPS-CuBP**, **TIPS-NiBP**) on a Rigaku CCD detector (Saturn 724) mounted on a Rigaku rotating anode X-ray generator (Micro-Max-007HF) using Mo-Kα radiation from the corresponding set of confocal optics. The structures were solved by direct methods and refined on F2 by full-matrix least-squares using the CrystalClear and SHELXS-2000 program. Ionization potential was determined by atmospheric photoelectron spectroscopy (Riken Keiki, AC-3). Materials **TMS-H_2CP** [17b], **TMS-ZnCP**, **TMS-ZnBP** [17c], **TIPS-H_2CP**, **TIPS-ZnCP** and **TIPS-ZnBP** [17a] were prepared according to the procedures described in literature. $PC_{71}BM$ was purchased from Luminescence Technology Corp. and used as received. Thermogravimetric analysis were performed on a Seiko Thermal Analyser Exstar TG/DTA 6200. X-ray diffraction (XRD) was recorded on a Rigaku Smartlab system. AFM image were recorded on Bruker D8 and Veeco Dimension Icon.

Synthesis

[5,15-Bis(trimethylsilylethynyl)tetrakis(bicycle[2,2,2]octadieno)porphyrinato]copper(II) (TMS-CuCP)

A saturated solution of $Cu(OAc)_2{\cdot}H_2O$ in methanol (18 mL) was added to a solution of **TMS-H_2CP** (0.118 g, 0.145 mmol) in $CHCl_3$ (50 mL). After stirring for 2 h at room temperature, the reaction mixture was poured into water and extracted with $CHCl_3$. The organic layer was washed with water and brine, then dried over Na_2SO_4, and the solvent was removed under a reduced pressure. The residue was purified by recrystallization $CHCl_3$ / MeOH to give **TMS-CuCP** as purple crystals in 84% (0.106 g, 0.121 mmol). UV–vis (CH_2Cl_2): λ_{max}, nm ($\varepsilon \times 10^4$): 431 (39.9), 563 (1.47), 591 (2.23),

605 (2.31); HRMS (ESI): m/z = 876.3119, calcd. for $C_{54}H_{53}N_4CuSi_2$: 876.3105 $[M + H]^+$. Elemental analysis: Anal. calcd for $C_{54}H_{52}CuN_4Si_2$: C, 73.98; H, 5.98; N, 6.39. Found: C, 73.92; H, 5.97; N, 6.41.

[5,15-Bis(trimethylsilylethynyl)tetrakis(bicycle[2,2,2]octadieno)porphyrinato]nickel(II) (TMS-NiCP)

A saturated solution of $Ni(OAc)_2{\cdot}4H_2O$ in methanol (10 mL) was added to a solution of **TMS-H_2CP** (0.113 g, 0.138 mmol) in $CHCl_3$ (50 mL) at room temperature. The mixture was refluxed for 3 h. After being cooled to room temperature, the reaction mixture was poured into water and extracted with $CHCl_3$. The organic layer was washed with water and brine, then dried over Na_2SO_4, and the solvent was removed under a reduced pressure. The residue was purified by recrystallization ($CHCl_3$/MeOH) to give **TMS-NiCP** as purple crystals in 87% (105 mg, 0.120 mmol). ^{1}H NMR (400 MHz; $CDCl_3$; Me_4Si): δ_H, ppm 9.55 (m, 2H), 6.97 (m, 8H), 6.35 (m, 4H), 5.39 (m, 4H), 2.04–1.83 (m, 16H), 0.57 (m, 18 H). ^{13}C NMR (100 MHz; $CDCl_3$; Me_4Si): δ_C, ppm 206.36, 151.68, 151.65, 151.59, 150.12, 150.02, 149.98, 137.16, 136.55, 136.53, 135.75, 133.36, 133.31, 106.28, 106.26, 106.20, 106.17, 98.10, 95.33, 77.20, 50.05, 38.90, 35.87, 27.25, 27.19, 27.01, 0.27, 0.09. UV–vis (CH_2Cl_2): λ_{max}, nm ($\varepsilon \times 10^4$): 430 (29.6), 603 (1.95); HRMS (ESI): m/z = 871.3168, calcd. for $C_{54}H_{53}N_4NiSi_2$: 871.3162 $[M + H]^+$. Elemental analysis: Anal. calcd for $C_{54}H_{52}N_4NiSi_2{\cdot}1/2\ H_2O$: C, 73.63; H, 6.06; N, 6.39. Found: C, 73.68; H, 5.96; N, 6.60.

[5,15-Bis(triisopropylsilylethynyl)tetrakis(bicycle[2,2,2]octadieno)porphyrinato]copper(II) (TIPS-CuCP)

A solution of $Cu(OAc)_2{\cdot}H_2O$ (407 mg, 2.04 mmol) in methanol (15 mL) was added to a solution of **TIPS-H_2CP** (101 mg, 0.103 mmol) in $CHCl_3$ (50 mL). After stirring for 2 h at room temperature, the reaction mixture was washed with saturated $NaHCO_3$ aq., and water. The mixture was then dried over Na_2SO_4, and the solvent was removed under reduced pressure. The residue was purified by recrystallization ($CHCl_3$/MeOH) to give **TIPS-CuCP** as purple crystals in 91% (97.7 mg, 0.0935 mmol). UV–vis (CH_2Cl_2): λ_{max}, nm ($\varepsilon \times 10^4$): 431 (41.1), 562 (1.74), 592 (2.64), 604 (2.47); HRMS (ESI): m/z = 1044.4984, calcd. for $C_{66}H_{77}Cu\ N_4Si_2$: 1044.4983 $[M + H]^+$.

[5,15-Bis(triisopropylsilylethynyl)tetrakis(bicycle[2,2,2]octadieno)porphyrinato]nic-kel(II) (TIPS-NiCP)

A solution of $Ni(OAc)_2{\cdot}4H_2O$ (0.507g, 2.04 mmol) in methanol (15 mL) was added to a solution of **TIPS-H_2CP** (101 mg, 0.103 mmol) in $CHCl_3$ (50 mL) at room temperature. The mixture was refluxed for 3 h. After being cooled to room temperature, the reaction mixture was washed with saturated $NaHCO_3$ aq., and water. The mixture was then dried over Na_2SO_4, and the solvent was removed under reduced pressure. The residue was purified by recrystallization ($CHCl_3$/MeOH) to give **TIPS-NiCP** as purple crystals in 93% (98.6 mg, 0.0948 mmol). ^{1}H NMR (400 MHz; $CDCl_3$; Me_4Si): δ_H, ppm 9.51 (m, 2H), 6.94 (m, 8H), 6.41 (m, 4H), 5.37 (m, 4H), 2.10–1.76 (m, 16H), 1.53–1.42 (m, 6H), 1.36–1.33 (m, 36H). ^{13}C NMR (100 MHz; $CDCl_3$; Me_4Si): δ_C, ppm 151.91, 151.87, 151.83, 151.80, 151.77, 150.55, 150.52, 150.50, 137.19, 137.15, 136.40, 136.38, 136.36, 135.90, 135.86, 135.82, 135.78, 133.06, 133.03, 107.28, 104.73, 104.66, 98.14, 95.30, 95.26, 38.66, 38.63, 35.90, 35.88, 27.23, 27.20, 27.15, 18.86, 11.78. UV–vis (CH_2Cl_2): λ_{max}, nm ($\varepsilon \times 10^4$): 432 (23.8), 594 (1.65), 601 (1.62). HRMS (ESI): m/z = 1039.5042, calcd. for $C_{66}H_{77}N_4NiSi_2$: 1039.5040 $[M + H]^+$.

5,15-Bis(trimethylsilylethynyl)tetrabenzoporphyrin (TMS-H_2BP)

TMS-H_2BP was prepared according to the procedures described in literature [17c]. Crystallographic data: $C_{46}H_{38}N_4Si_2$, Mw = 702.98, monoclinic, space group $C2/c$, a = 37.5744(10), b = 6.47957(16), c = 15.2073(4) Å, β = 100.5070(10), V = 3640.37(17) Å^3, T = 103 K, Z = 4, R_1 = 0.0478, wR_2 = 0.1282, GOF = 1.064, CCDC NO. 1031711.

[5,15-Bis(trimethylsilylethynyl)tetrabenzoporphyrinato]zinc(II) (TMS-ZnBP)

TMS-ZnBP was prepared according to the procedures described in literature [17c]. Crystallographic data: $C_{46}H_{36}N_4Si_2Zn$, Mw = 766.34, monoclinic, space group $C2/c$, a = 37.029(3), b = 6.5615(4), c = 15.1517(4) Å, β = 100.2749(15), V = 3610.6(4) Å^3, T = 103 K, Z = 4, R_1 = 0.0596, wR_2 = 0.1596, GOF = 1.030, CCDC NO. 1039260.

[5,15-Bis(trimethylsilylethynyl)tetrabenzoporphyrinato]copper(II) (TMS-CuBP)

TMS-CuCP was heated at 200 °C for 1 h in a sample tube under reduced pressure to give **TMS-CuBP** quantitatively. UV–vis (DMF): λ_{max}, nm ($\varepsilon \times 10^4$): 462 (38.6), 641 (3.27), 678 (7.81). HRMS (MALDI): *m*/*z* = 763.1769, calcd. for $C_{46}H_{36}CuN_4Si_2$: 763.1775 $[M]^+$. Crystallographic data: $C_{46}H_{36}CuN_4Si_2$, *Mw* = 764.54, monoclinic, space group *C*2/*c*, *a* = 37.0934(9), *b* = 6.5331(2), *c* = 15.2433(4) Å, β = 101.1999(7)°, *V* = 3623.6(2) Å^3, *T* = 103 K, *Z* = 4, R_1 = 0.0410, wR_2 = 0.1064, GOF = 1.069, CCDC NO. 1031710.

[5,15-Bis(trimethylsilylethynyl)tetrabenzoporphyrinato]nickel(II) (TMS-NiBP)

TMS-NiCP was heated at 200 °C for 1 h in a sample tube under reduced pressure to give **TMS-NiBP** quantitatively. ^{1}H and ^{13}C NMR spectra could not record because of the low solubility. UV–vis (DMF): λ_{max}, nm ($\varepsilon \times 10^4$): 462 (30.0), 642 (2.53), 677 (4.94). HRMS (MALDI): *m*/*z* = 758.1827, calcd. for $C_{46}H_{36}N_4NiSi_2$: 758.1832 $[M]^+$. Crystallographic data: $2(C_{46}H_{36}N_4NiSi_2)\cdot C_6H_5Cl$, *Mw* = 3146.27, triclinic, space group *P*-1, *a* = 13.9807(3), *b* = 17.5488(4), *c* = 18.7217(4) Å, α = 63.4700 (7), β = 76.3869(7), γ= 67.1216(7)°, *V* = 3775.7(2) Å^3, *T* = 103 K, *Z* = 1, R_1 = 0.0352, wR_2 = 0.0955, GOF = 1.091, CCDC NO. 1031712.

[5,15-Bis(triisopropylsilylethynyl)tetrabenzoporphyrinato]zinc(II) (TIPS-ZnBP)

TIPS-ZnBP was prepared according to the procedures described in literature [17a]. UV–vis (THF): λ_{max}, nm ($\varepsilon \times 10^4$): 468 (61.7), 632 (1.96), 647 (1.87), 681 (9.96). Crystallographic data: $C_{174}H_{180}N_{12}Si_6Zn_3$, *Mw* = 2083.95, triclinic, space group *P*-1, *a* = 12.9138(2), *b* = 15.6986(3), *c* = 19.0118(4) Å, α = 101.5960(10), β = 108.2190(10), γ= 97.6090(10), *V* = 3506.44(11) Å^3, *T* = 103 K, *Z* = 1, R_1 = 0.0476, wR_2 = 0.1275, GOF = 1.069, CCDC NO. 1040808.

[5,15-Bis(triisopropylsilylethynyl)tetrabenzoporphyrinato]copper(II) (TIPS-CuBP)

TIPS-CuCP was heated at 200 °C for 1 h in a sample tube under reduced pressure to give **TIPS-CuBP** quantitatively. UV–vis (CH_2Cl_2): λ_{max}, nm ($\varepsilon \times 10^4$): 682 (5.75), 642 (2.64), 463 (32.0), 314 (1.75). HRMS (ESI): *m*/*z* = 954.3551, calcd. for $C_{58}H_{60}CuN_4Si_2$: 954.3550 $[M]^+$. Crystallographic data: $C_{58}H_{60}CuN_4Si_2$, *Mw* = 932.82, triclinic, space group *P*-1, *a* = 12.9931(3), *b* = 15.6209(4), *c* = 19.0424(4) Å, α = 101.3190(10), β = 108.7220(10), γ = 97.5070(10)°, *V* = 3510.32(14) Å^3, *T* = 123 K, *Z* = 3, R_1 = 0.0410, wR_2 = 0.1006, GOF = 1.070, CCDC NO. 1031708.

[5,15-Bis(triisopropylsilylethynyl)tetrabenzoporphyrinato]nickel(II) (TIPS-NiBP)

TIPS-NiCP was heated at 200 °C for 1 h in a sample tube under reduced pressure to give **TIPS-NiBP** quantitatively. ^{1}H NMR (400 MHz; $CDCl_3$; Me_4Si): δ_H, ppm 9.98 (m, 4H), 8.97 (m, 2H), 8.71 (m, 4H), 7.91 (m, 4H), 7.81 (m, 4H), 1.53–1.43 (m, 6H), 1.38-1.32 (m, 36H). ^{13}C NMR (100 MHz; $CDCl_3$; Me_4Si): δ_C, ppm 138.25, 137.34, 136.58, 133.58, 126.19, 125.95, 124.66, 119.69, 108.51, 106.41, 94.18, 92.37, 18.96, 11.71. UV–vis (CH_2Cl_2): λ_{max}, nm ($\varepsilon \times 10^4$): 689 (4.51), 645 (2.48), 465 (22.6), 314 (2.08). HRMS (ESI): *m*/*z* = 927.3787, calcd. for $C_{58}H_{60}N_4NiSi_2$: 927.3788 $[M + H]^+$. Crystallographic data: $C_{58}H_{60}N_4NiSi_2$, *Mw* = 928.01, monoclinic, space group $P2_1/n$, *a* = 23.6378(5), *b* = 16.8788(3), *c* = 26.1340(5) Å, β = 113.5099(7)°, *V* = 9561.4(3) Å^3, *T* = 123 K, *Z* = 8, R_1 = 0.0363, wR_2 = 0.0965, GOF = 1.033, CCDC NO. 1031709.

Electrochemical measurements

CV and DPV measurements were conducted in a solution of 0.1 M *n*-Bu_4NPF_6 in CH_2Cl_2 (**TIPS-H_2BP**) or benzonitrile (**TIPS-ZnBP**, **TIPS-CuBP** and **TIPS-NiBP**) with a scan rate of 100 mV.s^{-1} at room temperature in an argon-filled cell. A glassy carbon electrode and a Pt wire were used as a working and a counter electrode, respectively. An $Ag/AgNO_3$ electrode was used as a reference electrode, which was normalized with the half-wave potential of ferrocene/ferrocenium cation (Fc/Fc^+) redox couple.

Fabrication and evaluation of organic thin-film transistor

The heavily doped *n*-type Si substrates with 300 nm thick thermally grown SiO_2 layer as the gate dielectric Si substrates were cleaned sequentially with H_2O, acetone and 2-propanol in an ultrasonic bath, and treated with UV-ozone plasma for 20 min. Chloroform solutions of precursors (**TMS-CPs** or **TIPS-CPs**, 7 mg.mL^{-1}) were spin coated at 1000 rpm for 40 sec on Si substrates in a nitrogen glove box, where H_2O and O_2 concentrations were < 0.5 ppm. **TIPS-CPs** or **TMS-CPs** films were annealed at 180 ºC for 30 min. Au source and drain electrodes (70 nm) were vacuum deposited through a metal shadow mask. The channel engeth (L) and width (W) were 50 μm and 5.5 mm, respectively.

Transfer (I_D–V_G) and output (I_D–V_D) curves of OTFT devices were measured using an Agilent HP4155C semiconductor parameter analyzer in a glove box at room temperature. Field-effect mobility (μ_{FET}) was estimated from the saturation regime at drain voltage V_{DS} = –100 V, using the equation:

$$I_{DS}=(\mu WC_i/2L)(V_G - V_{th})^2 \quad (1)$$

where I_{DS} is the drain-source current, μ the field-effect mobility, W the channel width, L the channel length, C_i the capacitance per unit area of the gate dielectric layer, and V_{th} the threshold voltage.

Fabrication and evaluation of organic cell

The typical spin-coated BHJ devices of **TIPS-H_2BP** or **TMS-H_2BP** and $PC_{71}BM$ [ITO/PEDOT:PSS (30 nm)/**TIPS-H_2BP**:$PC_{71}BM$ or **TMS-H_2BP**:$PC_{71}BM$/BCP (7 nm)/Al (100 nm)] were fabricated as follows; ITO-coated glass substrates were cleaned stepwisely in Semico clean 56, water, acetone, and 2-propanol under ultrasonication for 10 min each. After the UV/O_3 treatment for 20 min, the poly(3,4-ethylenedioxythiophene):poly(4-styrenesulfonate) layer (PEDOT:PSS, Clevios, Al4083) was spin-coated onto a cleaned ITO surface. After being baked at 120 °C in air for 20 min, the substrates were transferred into a nitrogen filled glove box (< 0.5 ppm O_2 and H_2O). **TIPS-H_2CP**:$PC_{71}BM$ = 1:1 (w/w) (10 mg.mL^{-1} chloroform:chlorobenzene = 1:1 (v/v), 250 μl, 800 rpm) or **TMS-H_2CP**:$PC_{71}BM$ = 1:1 (w/w) (20 mg.mL^{-1} chloroform, 250 μL, 2500 rpm) spin-coated for 40 sec. in a glove box, then heated at by the various temperatures for 30 min. followed by the continuous vacuum deposition of BCP (7 nm) and Al (100 nm). The device was then tested in air after the encapsulation in the glove box. The current–voltage (J–V) curves were measured using a Keithley 2400 source measure unit under AM 1.5G illumination at an intensity of 100 mW.cm^{-2} using a solar simulator (Bunko-keiki, CEP-2000TF). The external quantum efficiency (EQE) spectra were measured with a Xe lamp and monochromator using a CEP-2000 integrated system by Bunko-keiki Co.

Acknowledgements

This work was supported by a Grant-in-Aid (no. 25288092 and 22350083 to H.Y. and no. 25288113 to K. N.), the Green Photonics Project in NAIST and the program for promoting the enhancement of research universities in NAIST sponsored by the Ministry of Education, Culture, Sports, Science and Technology, Japan. We acknowledge the Nippon Synthetic Chem. Ind. (Osaka, Japan) for a gift of ethyl isocyanoacetate, which was used for the preparation of the starting pyrroles.

REFERENCES

1. Yuan Y, Giri G, Ayzner AL, Zoombelt AP, Mannsfeld SCB, Chen J, Nordlund D, Toney MF, Huang J and Bao Z. *Nat. Commun.* 2014; **5**: 3005.

2. Luo C, Kyaw AKK, Perez LA, Patel S, Wang M, Brimm B, Bazan GC, Kramer EJ and Heeger AJ. *Nano Lett*. 2014; **14**: 2764–2771.
3. Kan B, Zhang Q, Li M, Wan X, Wan N, Long G, Wang Y. Yang X, Feng H and Chen Y. *J. Am. Chem. Soc*. 2014; **136**: 15529–15532.
4. Ito S, Murashima T, Ono N and Uno H. *Chem. Commun*. 1998; 1661–1662.
5. a) Ono N, Yamada H and Okujima T. *Handbook of Porphyrin Science*, vol. 2. World Scientific: Singapore, 2010; 1–102. b) Carvalho CMBC, Brocksom TJ and Oliveira KT. *Chem. Soc. Rev*. 2013; **42**: 3302–3317 and reference sited therein. c) Roznyatovskiy VV, Lee C-H and Sessler JL. *Chem. Soc. Rev*. 2013; **42**: 1921–1933 and reference sited therein. d) Yamada H, Okujima T and Ono N. *Chem. Commun*. 2008; 2957–2974 and reference sited therein. e) Ishida S-i, Kuzuhara D, Yamada H and Osuka A. *Asia. J. Org. Chem*. 2014; **3**: 716–722.
6. Hirao A, Akiyama T, Okujima T, Yamada H, Uno H, Sakai Y,Aramaki S, and N Ono. *Chem. Commun*. 2008; **39**: 4714–4716.
7. a) Nakamura M, Kitatsuka M, Takahashi K, Nagata T, Mori S, Kuzuhara D, Okujima T, Yamada, H, Nakae T and Uno H. *Org. Biomol. Chem*. 2014; **12**: 1309–1317. b) Nakamura M, Tahara H, Takahashi K, Nagata T, Uoyama H, Kuzuhara D, Mori S, Okujima T, Yamada H and Uno H. *Org. Biomol. Chem*. 2012; **10**: 6840–6849. c) Tomimori Y, Okujima T, Yano T, Mori S, Ono N, Yamada H and Uno H. *Tetrahedron* 2011; **67**: 3187–3193. d) Okujima T, Tomimori Y, Nakamura J, Yamada H, Uno H and Ono N. *Tetrahedron* 2010; **66**: 6895-6900. e) Uno H, S. Ito S, Wada M, Watanabe H, Nagai M, Hayashi A, Murashima T and Ono N. *J. Chem. Soc., Perkin Trans*. 2000; **1**: 4347–4355.
8. a) Liu Q, Kong F-T, Tetsuo O, Yamada H, Dai S-Y, Uno H, Ono N, You X-Z and Shen Z. *Tetrahedron Lett*. 2012; **53**: 3264–3267. b) Liu Q, Feng Q-Y, Yamada H, Wang Z-S, Ono N, You X-Z and Shen Z. *Chem. Asia. J*. 2012; **7**: 1312–1319. c) Shimizu Y, Shen Z, Ito S, Uno H, Daubc J and Ono N. *Tetrahedron Lett*. 2002; **43**: 8485–8488.
9. Uno H, Moriyama K, Ishikawa T, Ono N, Yahiro H. *Tetrahedron Lett*. 2004; **45**: 9083–9086.
10. a) Tanaka K, Aratani N, Kuzuhara D, Sakamoto S, Okujima T, Ono N, Uno H and Yamada H. *RSC Adv*., 2013; **3**: 15310–15315. b) Herwig PT Mullen K. *Adv. Mater*. 1999; **11**: 480-483. c) Uno H, Takiue T, Uoyama H, Okujima T, Yamada H and Masuda G. *Heterocycles* 2010; **82**: 791–802.
11. Shea PB, Kanicki J. Pattison LR, Petroff P, Kawano M, Yamada H and Ono N. *J. Appl. Phys*. 2006; **100**: 034502.
12. Matsuo Y, Sato Y. Niinomi T, Soga I, Tanaka H and Nakamura E. *J. Am. Chem. Soc*. 2009; **131**: 16048–16050.
13. Tamura Y, Saeki H, Hashizume J, Okazaki Y, Kuzuhara D, Suzuki M, Aratani N and Yamada H. *Chem. Commun*. 2014; **50**: 10379–10381.
14. Anthony JE. *Chem. Rev*. 2006; **106**: 5028-5048 and reference sited therein.
15. Diao Y, Tee BC-K, Giri G, Xu J, Kim DH, Becerril HA, Stoltenberg RM, Lee TH, Xue G, Mannsfeld SCB and Bao Z. *Nat. Mater*. 2013; **12**: 665–671.
16. a) Bunz UHF, Engelhart JU, Lindner BD and Schaffroth M. *Angew. Chem. Int. Ed*. 2013; **52**: 3810–3821 and reference sited therein. b) Wang C, Dong H, Hu W, Liu Y and Zhu D. *Chem. Rev*. 2012; **112**: 2208-2267 and reference sited therein.
17. a) Takahashi K, Kuzuhara D, Aratani N and Yamada H. *J. Photopol. Sci. Tech*. 2013; **26**: 213–216. b) Yamada H, Kushibe K, Mitsuogi S, Okujima T, Uno H and Ono N. *Tetrahedron Lett*. 2008, **49**, 4731–4733. c) Yamada H, Kushibe K, Okujima T, Uno H and Ono N. *Chem. Commun*. 2006; 383–385.

18. a) Lin Y-F, Shu Y, Parkin SR, Anthony JE and Malliaras GG. *J. Mater. Chem.* 2009; **19**: 3049–3056. b) Payne MM, Parkin SR, Anthony JE, Kuo C-C and Jackson TN. *J. Am. Chem. Soc.* 2005; **127**: 4986–4987. c) Anthony JE, Eaton DL and Parkin SR. *Org. Lett.* 2002; **4**: 15–18.
19. Saeki H, Kurimoto O, Nakaoka H, Misaki M, Kuzuhara D, Yamada H, Ishida K and Ueda. *Y. J. Mater. Chem. C* 2014; 2: 5357–5364.
20. Peumans P, Yakimov Aharon and Forrest SR. *J. Appl. Phys.* 2003; **93**: 3693–3723 and reference sited therein.
21. Guide M, Lin JDA, Proctor CM, Chen J, García-Cervera C and Nguyen T-Q. *J. Mater. Chem. A,* 2014; **2**: 7890–7896.

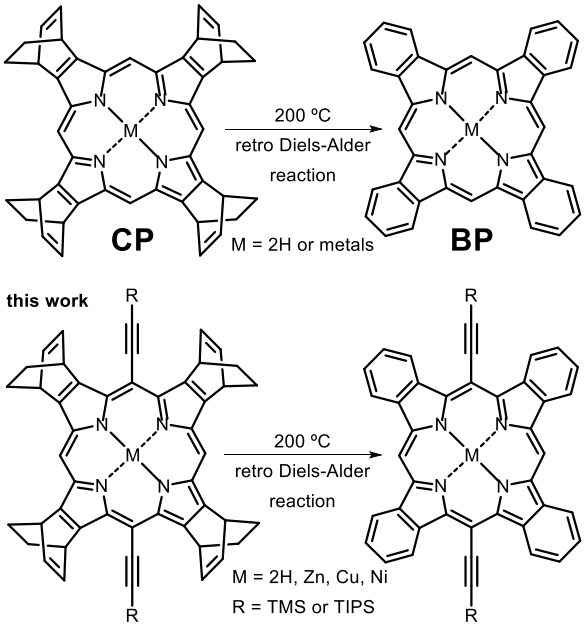

Fig. 1. Synthesis of **BP**s by the retro Diels–Alder reaction

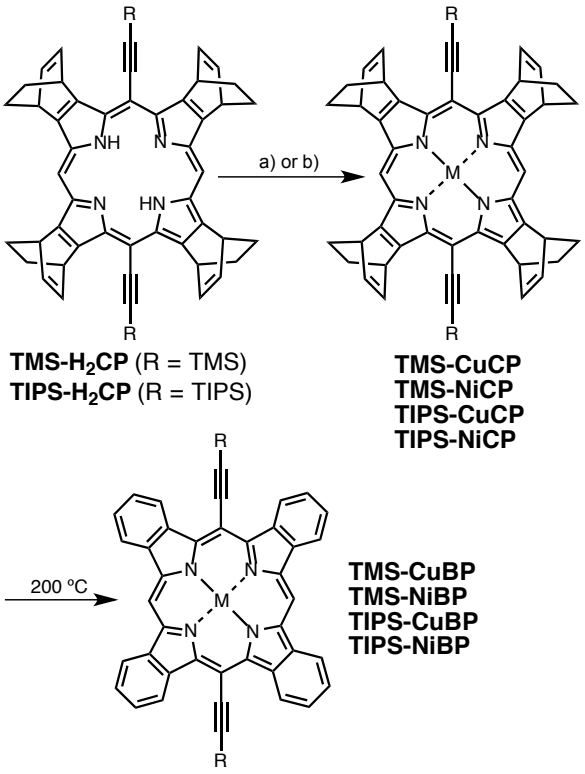

Scheme 1. Synthesis of **TMS**-**BP** and **TIPS**-**BP** metal complexes. Reagents and conditions: a) $Cu(OAc)_2 \cdot H_2O$, $CHCl_3$, MeOH; b) $Ni(OAc)_2 \cdot 4H_2O$, $CHCl_3$, MeOH

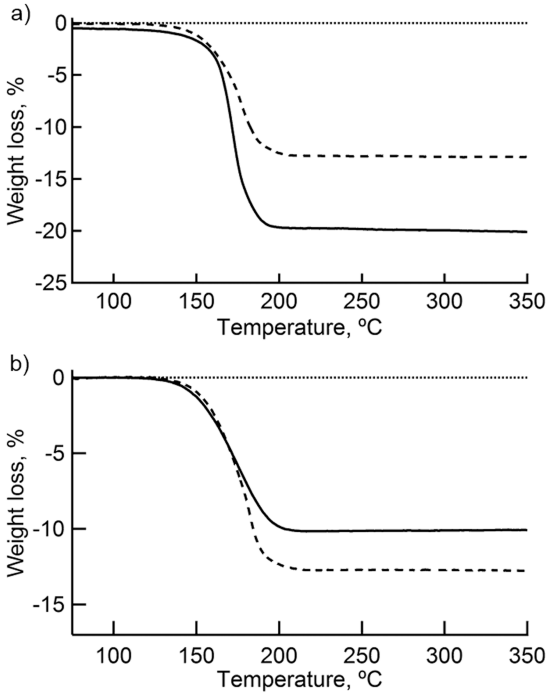

Fig. 2. Thermogravimetric analyses of a) **TMS**-**CuBP** (dotted line) and **TIPS**-**CuBP** (solid line), b) **TMS**-**NiBP** (dotted line) and **TIPS**-**NiBP** (solid line). Data was taken with a heating rate of 10 °C.min^{-1} under a nitrogen atmosphere

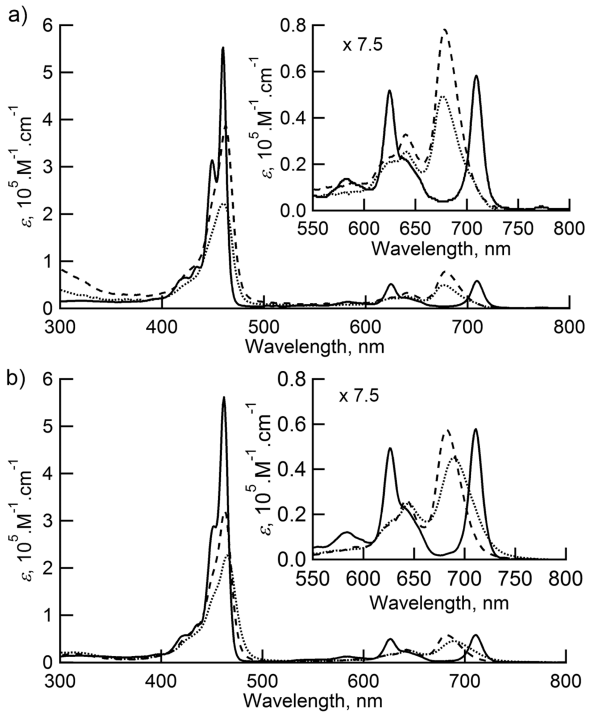

Fig. 3. Absorption spectra of a) **TMS**-**CuBP** (broken line), **TMS**-**NiBP** (dotted line) and **TMS**-**H_2BP** (solid line) in DMF and b) **TIPS**-**CuBP** (broken line), **TIPS**-**NiBP** (dotted line) and **TIPS**-**H_2BP** (solid line) in CH_2Cl_2

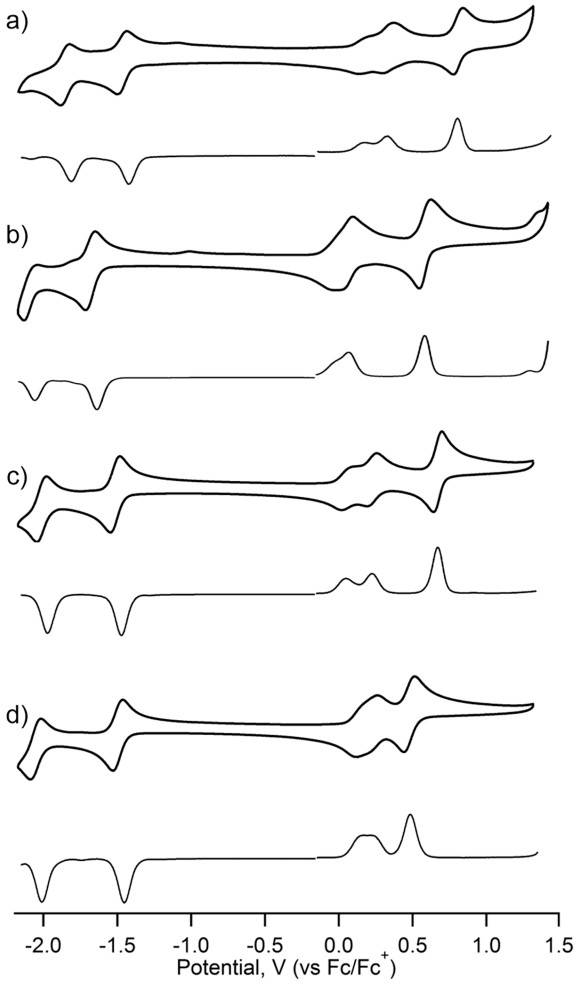

Fig. 4. Cyclic voltammograms (solid lines) and differential pulse voltammograms (thin lines) of a) **TIPS**-**H_2BP**, b) **TIPS**-**ZnBP**, c) **TIPS**-**CuBP** and d) **TIPS**-**NiBP** in CH_2Cl_2 for **TIPS**-**H_2BP**, in benzonitrile for **TIPS**-**ZnBP**, **TIPS**-**CuBP** and **TIPS**-**NiBP** with 0.1 M *n*-Bu_4NPF_6. Scan rate = 100 mV.s^{-1}

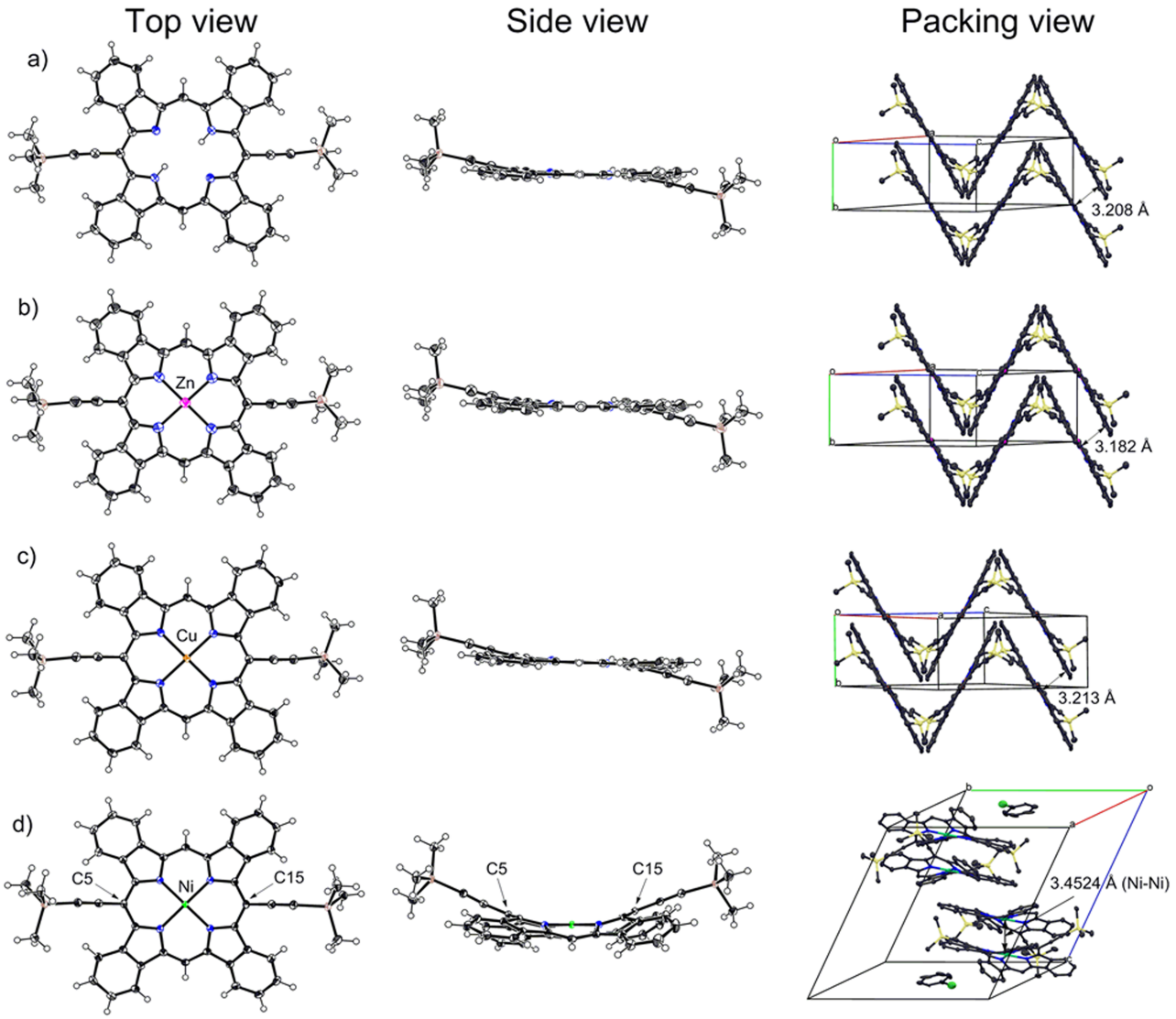

Fig. 5. Crystal structures of **TMS-H_2BP**, **TMS-ZnBP**, **TMS-CuBP** and **TMS-NiBP**. Top (left column) and side (center column) and packing (right column) views of a) **TMS-H_2BP**, b) **TMS-ZnBP** c) **TMS-CuBP** and d) **TMS-NiBP**. Thermal ellipsoids represent the 50% probability for top view and side view. Hydrogen atoms were omitted for clarity for packing view

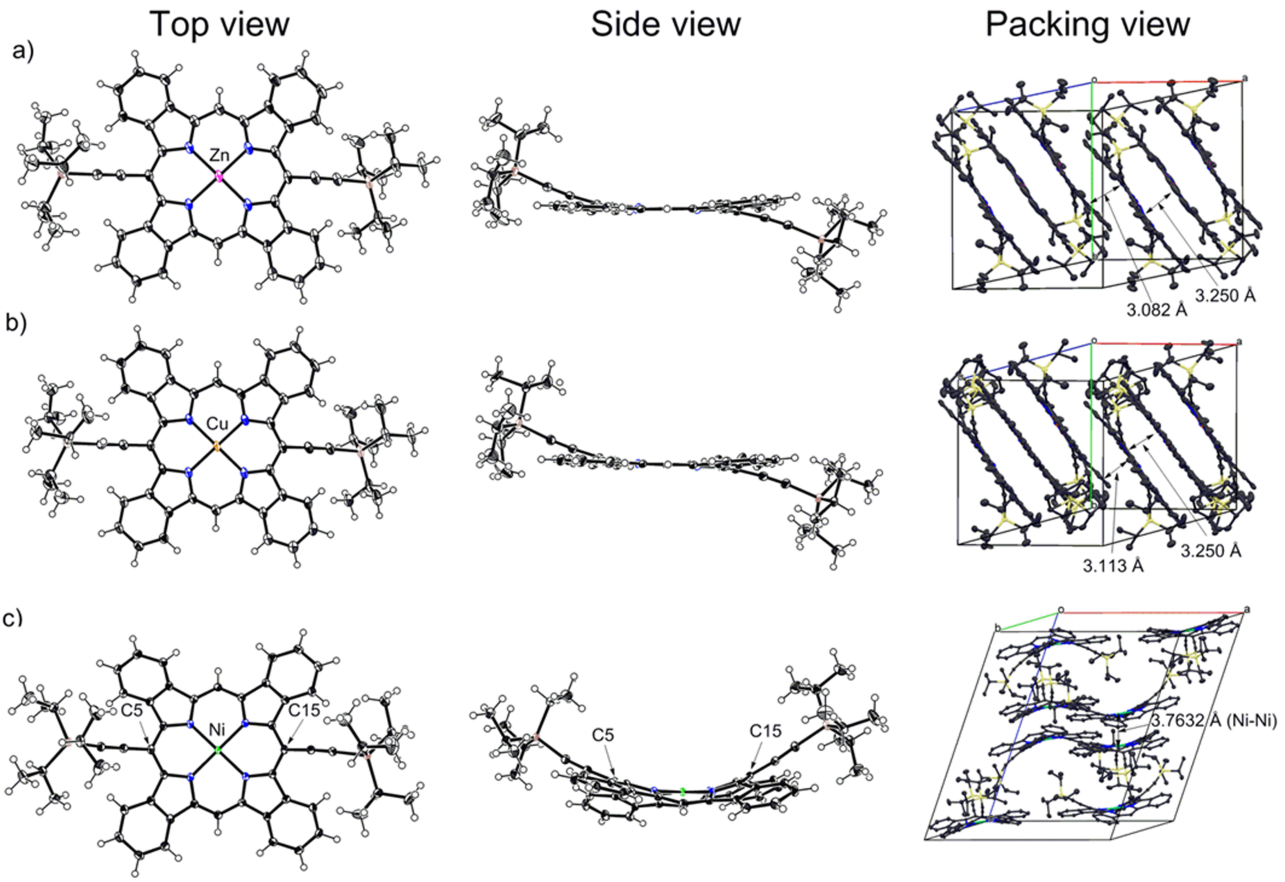

Fig. 6. Crystal structures of **TIPS**-**ZnBP**, **TIPS**-**CuBP** and **TIPS**-**NiBP**. Top (left column) and side (center column) and packing (right column) view of a) **TIPS**-**ZnBP**, b) **TIPS**-**CuBP** and c) **TIPS**-**NiBP**. Thermal ellipsoids represent the 50% probability for top view and side view. Hydrogen atoms were omitted for clarity for packing view

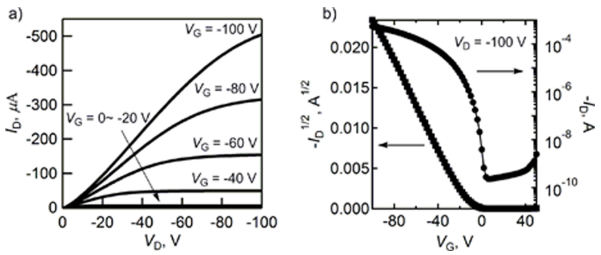

Fig. 7. OTFT characteristics of bottom-gate and top-contact device based on **TMS-H_2BP**. a) Out pot curves at different gate voltages. b) Transfer curves in the saturated region at a drain voltage of –100 V

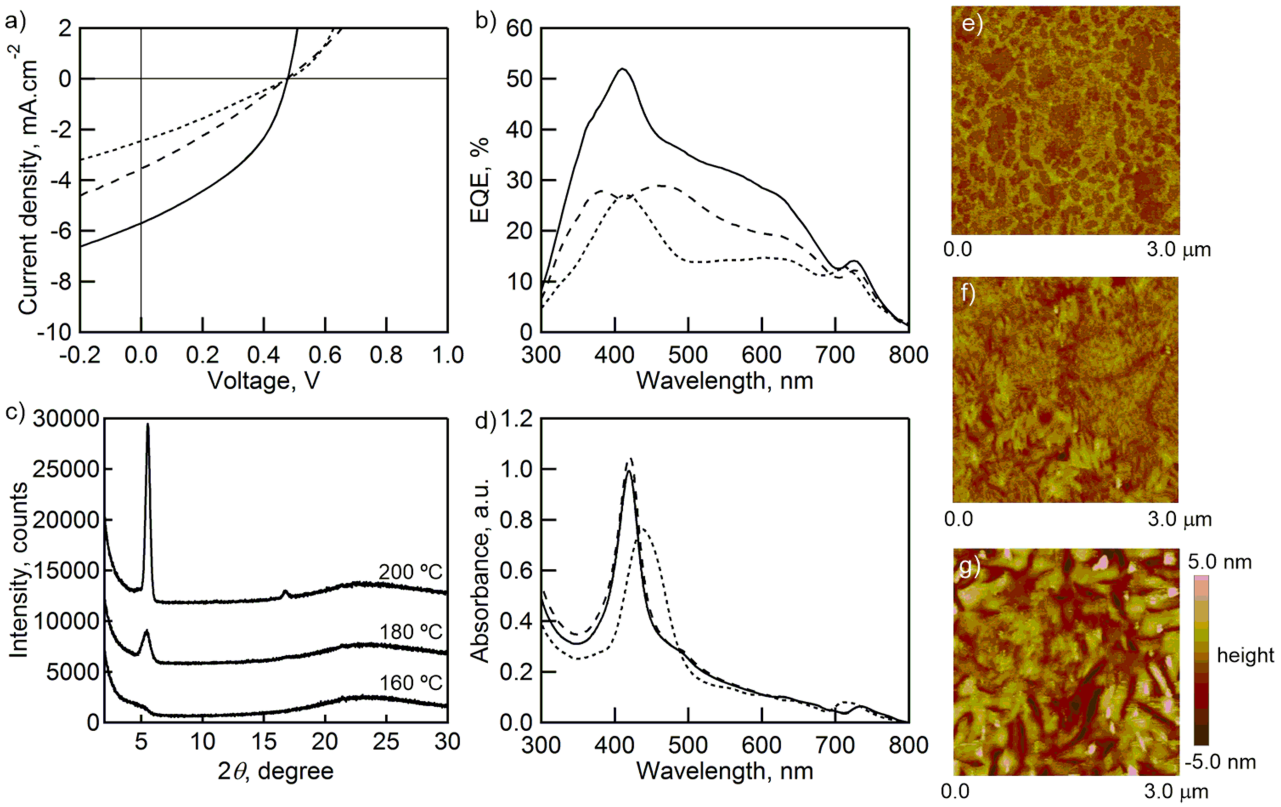

Fig. 8. a) *J–V* curves of BHJ solar cells based on **TMS-H$_2$BP**:PC$_{71}$BM produced at 160 (dotted), 180 (solid) and 200 °C (dashed). b) EQE spectra of BHJ solar cells based on **TMS-H$_2$BP**:PC$_{71}$BM produced at 160 (dotted), 180 (solid) and 200 °C (dashed). c) XRD patterns of **TMS-H$_2$BP**:PC$_{71}$BM composite films. d) Absorption spectra of **TMS-H$_2$BP**:PC$_{71}$BM film produced at 160 (dotted), 180 (solid) and 200 °C (dashed). Tapping-mode AFM height images of the **TMS-H$_2$BP**:PC$_{71}$BM composite films produced at e) 160, f) 180, and g) 200 °C

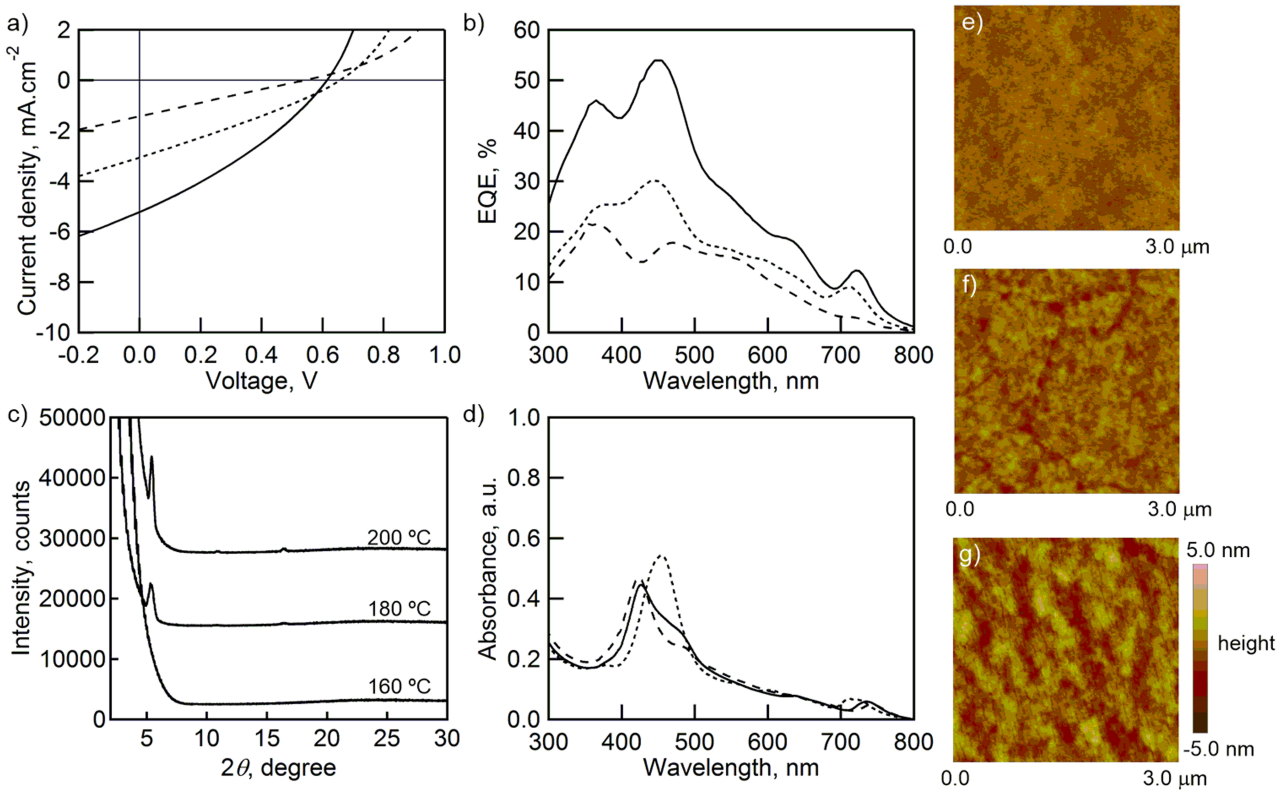

Fig. 9. a) *J–V* curves of BHJ solar cells based on **TIPS-H_2BP**:$PC_{71}BM$ produced at 160 (dotted), 180 (solid) and 200 ºC (dashed). b) EQE spectra of **TIPS-H_2BP**:$PC_{71}BM$ produced at 160 (dotted), 180 (solid) and 200 ºC (dashed). c) XRD patterns of **TIPS-H_2BP**:$PC_{71}BM$ composite films. d) Absorption spectra of **TIPS-H_2BP**:$PC_{71}BM$ films produced at 160 (dotted), 180 (solid) and 200 ºC (dashed). Tapping-mode AFM height images of the **TIPS-H_2BP**:$PC_{71}BM$ composite films produced at e) 160, f) 180, and g) 200 ºC

Table 1. Optical and electrochemical properties

Coumpounds	λ_{abs}, nm	E_{ox}, V [d]	E_{red}, V [d]	E_g, eV [e]	E_{HOMO}, eV [f]	E_{LUMO}, eV [g]
TMS-H_2BP	450, 460, 583, 625, 710 [a]	–	–	1.56	–5.18	–3.61
TMS-ZnBP	467, 633, 649, 682 [b]	–	–	1.60	–5.25	–3.62
TMS-CuBP	462, 641, 678 [b]	–	–	1.61	–5.10	–3.49
TMS-NiBP	462, 642, 677 [b]	–	–	–	–	–
TIPS-H_2BP	452, 462, 583, 626, 711 [a]	0.18, 0.34, 0.81	–1.42, –1.81	1.59	–5.20	–3.61
TIPS-ZnBP	468, 632, 647, 681 [c]	0.08, 0.59	–1.64, –2.06	1.61	–5.37	–3.76
TIPS-CuBP	463, 642, 682 [a]	0.06, 0.23, 0.68	–1.34, –1.48	1.62	–4.88	–3.26
TIPS-NiBP	465, 645, 689 [a]	0.17, 0.22, 0.37	–1.30, –2.01	–	–	–

[a] in CH_2Cl_2, [b] in DMF, [c] in THF, [d] Potential values were measured by DPV in CH_2Cl_2 for **TIPS-H_2BP**, in benzonitrile for **TIPS-ZnBP**, **TIPS-CuBP** and **TIPS-NiBP** with 0.1 M *n*-Bu_4NPF_6. The ferrocene/ferrocenium cation redox couple was used as the internal standard. Scan rate = 100 mV.s^{-1}. [sample] = 0.5 mM. Working electrode: glassy carbon. Counter electrode: Pt wire. Reference electrode: $Ag/AgNO_3$. [e] Determined by optical gaps from the absorption onsets in the films. [f] Determined by photoelectron spectroscopy in air. [g] $E_{LUMO} = E_{HOMO} + E_g$

Table 2. OTFT characteristics of **TMS-** and **TIPS-BP**s.

Compounds	μ_{FET}, $cm^2.V^{-1}.s^{-1}$	I_{on} / I_{off}	V_{th}, V
TMS-H_2BP	0.11	2.4×10^6	–12.3
TMS-ZnBP	5.56×10^{-5}	8.0×10^1	19.4
TMS-CuBP	4.49×10^{-4}	9.4×10^4	–11.9
TIPS-H_2BP	4.36×10^{-5}	4.3×10^4	–17.8
TIPS-ZnBP	1.11×10^{-5}	6.6×10^3	1.2
TIPS-CuBP	5.61×10^{-3}	1.9×10^4	–12.2

Table 3. Device performances of **TMS-** and **TIPS-BP-**based OSCs

p-type materials	Temperature, ºC	J_{SC}, mA.cm^{-2}	V_{OC}, V	FF	PCE, %
TMS-H$_2$BP	160	2.46	0.48	0.28	0.33
	180	5.70	0.48	0.40	1.09
	200	3.53	0.47	0.28	0.47
TMS-ZnBP	160	6.79	0.45	0.37	1.13
	180	7.81	0.46	0.41	1.49
	200	7.86	0.47	0.39	1.44
TMS-CuBP	160	4.51	0.43	0.38	0.72
	180	1.83	0.43	0.18	0.14
	200	1.49	0.42	0.30	0.19
TIPS-H$_2$BP	160	3.06	0.66	0.29	0.57
	180	5.22	0.61	0.32	1.02
	200	1.43	0.54	0.24	0.19
TIPS-ZnBP	160	2.12	0.68	0.30	0.44
	180	5.03	0.61	0.37	1.13
	200	4.29	0.64	0.36	0.99
TIPS-CuBP	160	3.85	0.65	0.34	0.86
	180	3.22	0.37	0.28	0.33
	200	3.64	0.42	0.28	0.42